Inorganic Chemistry

ARTICLE

pubs.acs.org/IC

Highly Linear Self-Assembled Porphyrin Wires

Matthieu Koepf,[†,‡] Jonas Conradt,[§] Jędrzej Szmytkowski,[§,⊥] Jennifer A. Wytko,*[,†] Lionel Allouche,[†] Heinz Kalt,[§] Teodor Silviu Balaban,[∥] and Jean Weiss*[,†]

[†]Institut de Chimie, UMR 7177 CNRS-UDS, 1 Rue Blaise Pascal, 67008 Strasbourg, France

[§]Institut für Angewandte Physik, Karlsruhe Institute of Technology (KIT), 76128 Karlsruhe, Germany

[∥]Université Paul Cézanne Aix-Marseille III, Institut de Sciences Moléculaires de Marseille, Chirosciences, UMR 6263, 13397 Marseille, France

Supporting Information

ABSTRACT: An efficient noncovalent assembly process involving high geometrical control was applied to a linear bis(imidazolyl zinc porphyrin) **7Zn**, bearing C_{18} substitutents, to generate linear multiporphyrin wires. The association process is based on imidazole recognition within the cavity of the phenanthroline-strapped zinc porphyrin. In chlorinated solvents, discrete soluble oligomers were obtained after $(\mathbf{7Zn})_n$ was end-capped with a terminal single imidazolyl zinc porphyrin derivative **4Zn**. These soluble species, as well as their destabilization in the presence of protic solvents, were studied by UV−visible and time-resolved luminescence. In the solid state, assemblies as long as 480 nm, which corresponds to 190 iterative units or a total of 380 porphyrins, were observed by atomic force microscopy measurements on mica. The length and linearity of the porphyrin wires obtained illustrate the potential of phenanthroline-strapped porphyrins for the directional control of self-assembly processes.

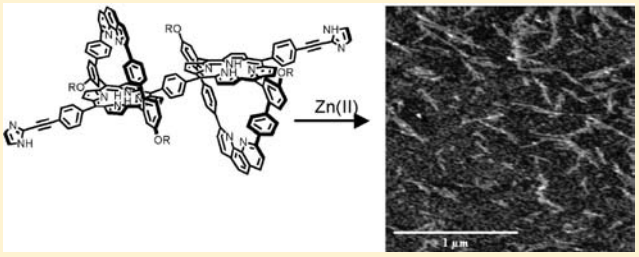

INTRODUCTION

In the development of nanomaterials for molecular electronics, porphyrin oligomers have received a great deal of attention in the past decade. Many examples of photoinduced energy- or electron-transfer reactions have been reported in geometrically well-defined porphyrin dyads, triads, and higher oligomers, providing crucial information on the energy- and electron-transfer mechanisms involved in these processes.[1] To produce large multiporphyrinic assemblies for future applications, the strong emergence of self-assembled multiporphyrinic species is extremely attractive.[2] Two main types of arrangements can be expected for multiporphyrin assemblies, namely, H-aggregates, with π-stacked porphyrins facing each other, and J-aggregates, with a partially overlapped side by side arrangement that is reminiscent of natural light harvesting antennae systems.[1,2] Many reported self-assembled scaffolds, inspired by H-aggregates, demonstrate the bright future of self-assembly. The mechanical resistance of assemblies that rely exclusively on aromatic stacking needs to be reinforced in various manners such as interactions of lipophilic side chains,[3] ion binding,[4] or hydrogen bonding.[5] For multiporphyrins of the J-aggregate type, a major issue concerns the linearity of the scaffolds.

A necessary step prior to the development of materials is the achievement of a high degree of linearity resembling that observed in polymer-type assemblies where linearity may originate from cohesion forces.[6,7] Aside from crystalline nanorods,[8] the largest multiporphyrinic assemblies reported were obtained by both covalent and self-assembled approaches, using respectively Osuka's[9] iterative oxidative coupling of meso-unsubstituted porphyrins, or Kobuke's[10] imidazole coordination in self-complementary zinc porphyrin dimers. These elegant and powerful approaches led to large multiporphyrin assemblies for which near-field microscopy imaging was reported.[11,12] In both covalent and self-assembled species, imaging showed that the linearity of the objects was inversely related to the size of the linear assembly.

The specific binding of *N*-unsubstituted imidazoles within the pocket of phenanthroline-strapped zinc porphyrins has been established and used as an assembly tool for photonic dyads and triads over the past few years.[13] Coordination of imidazole within the phenanthroline pocket is enhanced by the combination of three noncovalent interactions: (1) a metal−ligand coordination bond, (2) $\pi-\pi$ stacking between the imidazole and the phenyl substituents on the phenanthroline, and (3) hydrogen bonding of imidazole's NH proton to phenanthroline's nitrogen atoms. Imidazolyl zinc porphyrins **3Zn** and **4Zn** assemble into linear wires under certain conditions on highly ordered pyrolytic graphite (HOPG).[14] To ensure the formation of continuous linear wires, two of these imidazolyl-porphyrins have now been

Received: January 19, 2011
Published: June 07, 2011

Scheme 1. Synthesis of the Self-Complementary Bis(imidazolyl porphyrin) 7Zn[a]

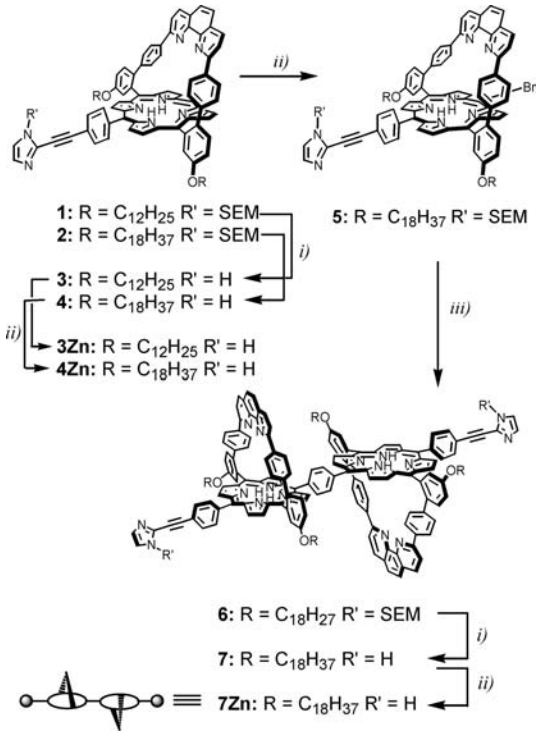

[a] (i) $(n\text{-Bu})_4NF$, THF, 50 °C; **3**, 56%; **4**, 63%; **7**, 48%. (ii) $Zn(OAc)_2$, THF, 60 °C, quantitative. (iii) (a) NBS, $CHCl_3$, 0 °C; (b) acetone; 100%; (c) 1,4-phenyldiboronic acid, $Pd(PPh_3)_4$ K_2CO_3, toluene, MeOH, H_2O, 60 °C; **6**, 65%.

linked by a phenyl spacer in the bis-porphyrin **7**. In the presence of zinc, after assembly at one end, the other end is still available to continue the oligomerization/polymization process. Solubility of the assemblies will be the size-limiting factor. Dissociation studies, photophysical measurements, and atomic force microscopy (AFM) images demonstrate the existence of **7Zn** as self-assembled filaments.

RESULTS AND DISCUSSION

Synthesis. Compounds **1** and **2** (Scheme 1) were prepared[14] by combining two synthetic approaches that lead to soluble phenanthroline-strapped porphyrins bearing long alkyl chains and to self-complementary imidazolyl-substituted porphyrins. Bromination[15] of the unsubstituted meso position afforded **5** quantitatively. A final coupling of 2 equiv of **5** with 1,4-phenyldiboronic acid afforded the protected bis-porphyrin **7**. Removal of the $CH_2OCH_2CH_2SiMe_3$ (SEM) protecting groups on **6** gave compound **7** in 48% yield.

Metalation of **7** with zinc acetate resulted in the precipitation of the deep green zinc derivative **7Zn**. Despite the presence of two long alkyl chains, this compound was insoluble in chlorinated solvents, toluene, alcohols, dimethylformamide (DMF), and dimethyl sulfoxide (DMSO). Compound **7Zn** was partially soluble in pyridine. For similar self-assembling systems, this type of behavior was attributed to the formation of very large species that precipitate at a critical size.[16−18] Mass spectroscopy of dilute samples of **7Zn** showed no trace of nonmetalated porphyrin; therefore, metalation was assumed to be quantitative.

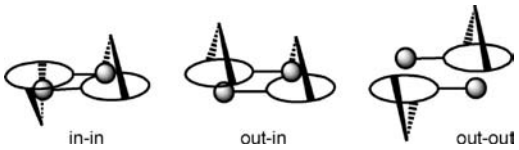

Figure 1. Three possible association modes for the homodimers $(\mathbf{3Zn})_2$ and $(\mathbf{4Zn})_2$. Alkyl chains are omitted for clarity. The terms "in" and "out" denote respectively whether the imidazole is bound within the phenanthroline pocket or outside of the phenanthroline pocket, at the distal site.

Assembly in Solution. Three possible modes of assembly can be envisioned for $(\mathbf{3Zn})_2$ and $(\mathbf{4Zn})_2$ (Figure 1). These modes differ by binding of imidazole either within the phenanthroline strap (denoted as "in") or on the distal, unhindered side of the porphyrin (denoted "out"). Semiempirical and molecular mechanics calculations in the gas phase indicated that although the in−out configuration is slightly preferred, there is little difference (<3 kcal) between the relative heats of formation of the three configurations (see the Supporting Information). Thus, in theory, three forms of the dimer can be engaged in a configurational equilibrium in solution.

As shown in Figure 2, the dimer $(\mathbf{3Zn})_2$ exhibited a rather simple set of ^1H NMR resonances that can only emerge from a unique and highly symmetrical arrangement. An in−out assembly was therefore eliminated as a possible conformation in solution. Compared to the free base porphyrin **3**, the doublet of the ortho (H_o) protons of the phenyl ring of the phenanthroline strap was shifted upfield from 6.68 ppm in the free base to 6.38 ppm in the zinc porphyrin. This shift, which results from a $\pi-\pi$ interaction between the imidazole and the phenyl ring bearing H_o, is characteristic of imidazole binding within the phenanthroline strap.[19] Only the in−in conformer accounts for the upfield shift of the H_o peak.

The apparent discrepancy between the rather imprecise theoretical calculations and the preferred configuration observed by NMR needs higher level calculations to be clarified, in view of the small differences involved. Particularly intriguing is that an X-ray structure of a phenanthroline-strapped zinc porphyrin−imidazole complex showed that the imidazole's NH hydrogen formed a bifurcated hydrogen bond with both nitrogen atoms of the phenanthroline.[19] In the X-ray analysis, this particular NH was positioned on the basis of the presence of electronic density; therefore, in our calculations, the prediction that the imidazole's NH hydrogen prefers a single hydrogen bond to only one of the phenanthroline's nitrogen atoms may be an artifact of the force field calculation. However, the preferred in−in configuration observed by NMR is easily explained by the formation of two hydrogen bonds that are highly favored by the use of chloroform as solvent.

Altogether, ^1H NMR clearly indicates that the self-complementary dimer $(\mathbf{3Zn})_2$ suffers some conformational mobility restraints due to stacking of the phenyl groups of both phenyl−ethynyl spacers. In the absence of zinc, the phenyl spacer located at the porphyrin's meso position in the free base monomer showed broad signals at 8.4 and 7.6−7.8 ppm, which suggest a precluded or slow free rotation around the imidazole−porphyrin axis. After zinc insertion and formation of the in−in dimer, the nearly face-to-face position of the two phenyl−ethynyl groups (see Figure 2 or the Supporting Information) is now fixed. The phenyl protons appear as two, well-defined sets of

dx.doi.org/10.1021/ic2001255 |Inorg. Chem. 2011, 50, 6073–6082

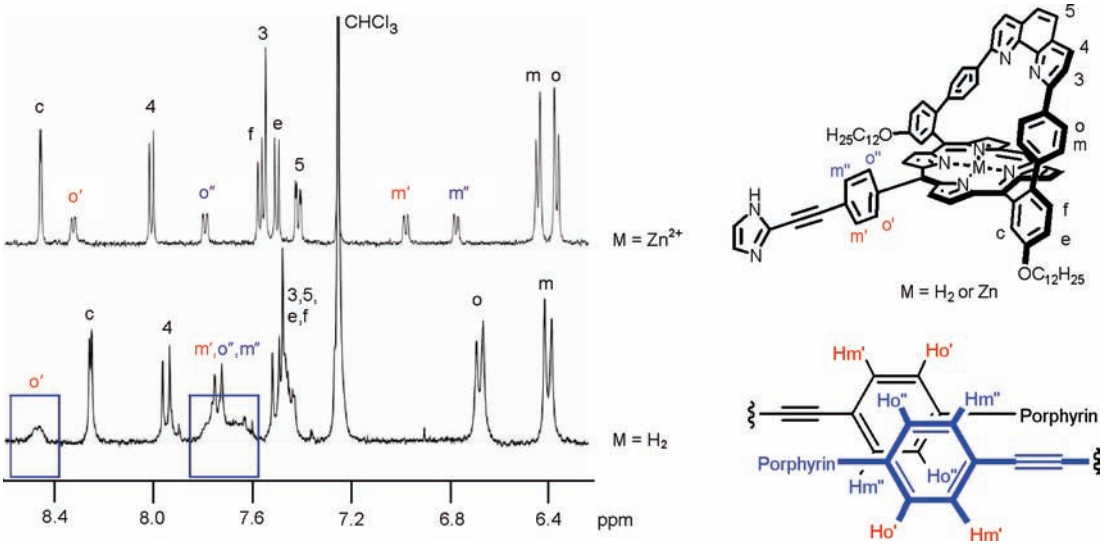

Figure 2. ^{1}H NMR spectra of **3** (bottom, 300 MHz) and **3Zn** (top, 500 MHz) in $CDCl_3$ ($\sim 5 \times 10^{-4}$ M). The phenyl protons of the phenyl-ethynyl bridge are boxed for the free base **3**.

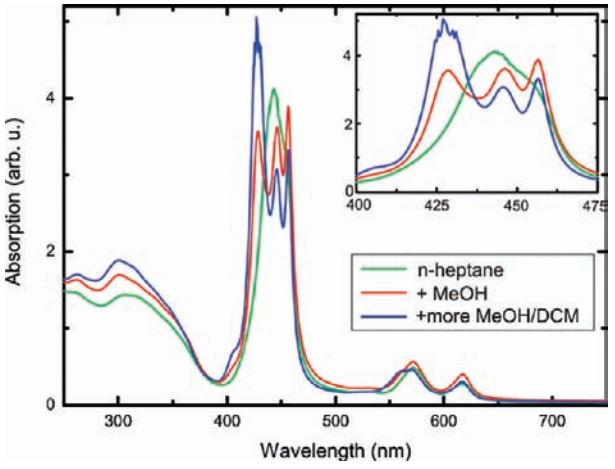

Figure 3. Absorption spectra of **4Zn** (dissolved in CH_2Cl_2 and then diluted with *n*-heptane to a concentration of 1×10^{-5} M) and changes upon addition of MeOH: red line, ~12 000 equiv of MeOH; blue line, ~36 000 equiv of MeOH plus enough CH_2Cl_2 (DCM) to obtain a homogeneous solution.

AX peaks at 8.34, 7.79, 6.98, and 6.78 ppm. Whereas the positions of the first two doublets are nearly unchanged, the latter two doublets are shifted upfield compared to the broad peaks in the free base precursor. The COSY NMR spectrum showed one correlation for the doublets at 8.34 and 6.98 ppm and another for the doublets at 7.79 and 6.78 ppm (see the Supporting Information). Thus, the first two doublets correspond to protons on the same side of the phenyl ring and the latter two correspond to the protons on the opposite side of the phenyl ring. The peaks at 8.34 and 7.79 ppm were attributed to $H_{o'}$ and $H_{o''}$ on the basis of a correlation in the NOESY spectrum between both of these doublets and the β_1 protons of the porphyrin ring (see the Supporting Information). The peak that is more upfield, at 7.79 ppm, was assigned to $H_{o''}$ because this proton is shielded by the electronic density of the phenyl ring of the second molecule in the dimer (see schematic representation in Figure 3 and the molecular model in Supporting Information Figure S3). Consequently, on the basis of the COSY NMR correlations, $H_{m'}$ and $H_{m''}$ were assigned to the doublets at 6.98 and 6.78 ppm, respectively. The larger upfield shifts of $H_{o''}$ and $H_{m''}$ are explained by molecular modeling that clearly places these protons at the van der Waals contact of the slightly offset neighboring phenyl linker (see Figure 2 and the Supporting Information). Particularly close proximities were calculated for $H_{o''}$ and $H_{m''}$ of one molecule respectively with $H_{m''}$ and $H_{o''}$ of the second molecule (respective distances of ca. 3.43 and 3.46 Å). All distances between other protons on opposite molecules are greater than 4.5 Å.

The formation of only a dimeric species was confirmed by DOSY ^{1}H NMR for 5×10^{-4} M solutions of **3Zn** and **4Zn** in $CDCl_3$ (D = 300 $\mu m^2/s$ for **3Zn** and 250 $\mu m^2/s$ for **4Zn**, 298 K).[14] These dimers are extremely stable with a self-association constant of 10^9 M^{-1} in $CHCl_3$ at 298 K. Dimers of **3Zn** and **4Zn** assemble into J-aggregates in *n*-heptane solution at 10^{-5} M.[14] The absorption spectrum of **4Zn** dissolved in a minimum of dichloromethane and then diluted with *n*-heptane is shown in Figure 3. The spectra shown in Figure 3 were measured at relatively high concentration (1×10^{-5} M) to favor aggregation; nevertheless, the absorptions remain in the linear response domain of the detector. The broad Soret band has a λ_{max} at 443 nm with a shoulder around 456 nm. The former absorption was attributed to the dimer and the latter to J-aggregates. To dissociate the dimers and aggregates, methanol was added (1 pipet drop or ~12 000 equiv), causing the Soret band to split into three distinct components with λ_{max} at 428, 446, and 456 nm. The absorption at 428 nm became more intense upon the addition of more MeOH (~36 000 equiv total), suggesting that this band corresponds to monomers coordinated by MeOH. The lower energy absorptions at 446 and 456 nm were thus respectively attributed to dimeric species and to aggregates. Assignment of these bands was confirmed by time-resolved photoluminescence studies (vide infra).

The in−in mode of coordination in $(\mathbf{4Zn})_2$ was also assumed for solution assembly of the bis(imidazolyl-porphyrin) **7Zn**. Due to its insolubility in noncoordinating solvents, ^{1}H NMR (300 MHz) of the bis-porphyrin **7Zn** could not be obtained in chlorinated solvents. However, **7Zn** was soluble in pyridine, which is a

dx.doi.org/10.1021/ic2001255 |*Inorg. Chem.* 2011, 50, 6073–6082

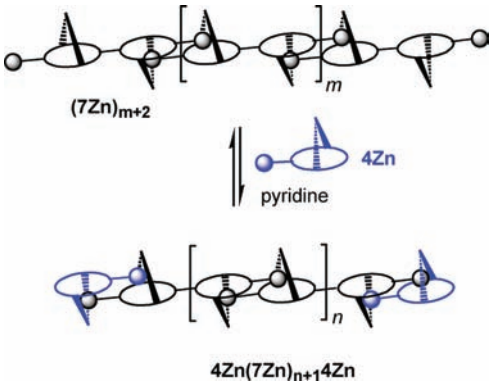

Figure 4. Dissociation of polymers of **7Zn** by addition of **4Zn**.

competitor for axial binding to zinc. The ^{1}H NMR (500 MHz) spectrum of **7Zn** in pyridine-d_5 showed sharp peaks (see Supporting Information) and only monomeric **7Zn** was observed in DOSY experiments of this sample.

To establish the existence of **7Zn** as self-assembled polymers, an experiment was carried out to dissociate the presumably long species into smaller segments by adding **4Zn** as an end-capping group, as schematically depicted in Figure 4. Bis(porphyrin) **7Zn** was dissolved in pyridine, and a small quantity (0.05 or 0.025 equiv) of **4Zn** was added. The solution was then equilibrated at 80 °C for 30 min. After removal of the pyridine under reduced pressure and vacuum drying for 12−15 h, 0.4 mL of $CDCl_3$ was added. This process was repeated until the solid completely dissolved in the 0.4 mL of $CDCl_3$. A soluble oligomer was obtained after the addition of 0.125 equiv of **4Zn**. The stoichiometry reached at this point for the dissolved species was theoretically seven molecules of **7Zn** to two molecules of **4Zn**.

The ^{1}H MNR (300 MHz, $CDCl_3$) of this mixture of **7Zn**/**4Zn** showed numerous broad peaks as well as some sharper peaks that could be assigned (see the Supporting Information). By comparing the integration of the meso porphyrin peak (10.23 ppm) of **4Zn** to that of the imidazole's H5 (4.31 ppm) present in both **4Zn** and **7Zn**, the ratio of **7Zn**/**4Zn** was estimated to be seven molecules of **7Zn** for two molecules of **4Zn**. Thus, the NMR estimation was in agreement with the initial stoichiometry, and the average distribution of end-capped oligomers observed in solution was centered around scaffolds with formula of **4Zn**-(**7Zn**)$_7$**4Zn** comprising 16 porphyrins. As shown by the spectrum of the soluble material, residual pyridine seemed to be absent from the solution. Although traces of pyridine may be considered, in dichloromethane, the large difference between the $\log K_{im} = 6.1$ and $\log K_{py} = 3.3$ on a phenanthroline-strapped zinc porphyrin[20,21] renders the binding of pyridine ineffective at NMR concentrations.

The length of these species could not be confirmed by DOSY experiments, however, because initially homogeneous solutions of **4Zn**(**7Zn**)$_7$**4Zn** in $CDCl_3$ precipitated within 22 h. Considering that the assembly is an equilibrium process, the solution of **7Zn**/**4Zn** does not exist as only end-capped hexamers or heptamers. Rather, oligomers or polymers of various lengths coexist in solution and species longer than approximately 16 porphyrins precipitate, which displaces the equilibrium toward the formation of insoluble oligomers **4Zn**(**7Zn**)$_{m+n}$**4Zn** and shorter, soluble species (see Supporting Information for a schematic representation). The DOSY experiment did show the existence of a species with a diffusion coefficient of 120 $\mu m^2/s$ ($CDCl_3$, 298 K), which corresponds to a monomer of **7Zn** end-capped with **4Zn**, i.e., **4Zn**(**7Zn**)**4Zn**.

In hopes of favoring oligomers shorter than **4Zn**(**7Zn**)$_7$**4Zn**, which might be observed by DOSY NMR, more **4Zn** was added, for a total of 22.5% of **4Zn** with respect to **7Zn**. The ^{1}H NMR ($CDCl_3$) spectrum of this solution, which corresponds to **4Zn**-(**7Zn**)$_4$**4Zn** on the basis of stoichiometry, was similar to that of **4Zn**(**7Zn**)$_7$**4Zn**. Unfortunately, precipitation began within 20 min of preparing the $CDCl_3$ solution of **4Zn**(**7Zn**)$_4$**4Zn**. Thus, a DOSY experiment was not carried out. More dilute solutions remained homogeneous for longer periods of time and were used for photophysical studies.

Photophysics. To verify the assignment of the absorption bands of **3Zn** or **4Zn**, time-resolved photoluminescence studies were carried out on solutions of **3Zn** or **4Zn** that were dissolved in a minimum amount of CH_2Cl_2 and then diluted with *n*-heptane to favor the formation of J-aggregates. The behavior of both compounds was similar; therefore, results representative of both compounds are described only for **4Zn**. Time-resolved spectra and decay-associated emission spectra (DAES) of **3Zn** are available as Supporting Information.

Upon excitation at 440 nm, two emission bands were observed at 620 and 672 nm (Figure 5a). The emission dynamics were best fit using the decay-associated emission spectra with two spectral components with different associated decay times (Figure 5b). The slow component decayed with $\tau_1 = 950$ ps and the fast one with $\tau_2 = 250$ ps. On the basis of other time-resolved investigations,[22,23] the former should correspond to the fluorescence of smaller species and the latter to fluorescence of larger aggregates. These decay times have to be compared to the reported 2.2 ns of an imidazole inclusion complex with a simple phenanthroline-strapped zinc porphyrin in pure CH_2Cl_2.[24] In **4Zn**, the observed slow component is more than two times faster than that of the simple phenanthroline-strapped zinc porphyrin; therefore, the 950 ps decay time is more likely due to a dimeric form of **4Zn**. The two spectral components of the DAES (Figure 5b) for these two decay times are of nearly equal amplitude, meaning that both dimers and oligomers/aggregates contribute equally to the fluorescence. These findings seem reasonable given that both dimers and oligomers/aggregates absorb at the excitation wavelength of 440 nm.

Upon excitation at 445 nm, the emission maxima remained the same at 620 and 670 nm (Figure 5c). A biexponential decay best fit the time-resolved spectrum. The decay times (see Table 1) were similar to those for excitation at 440 nm and were assigned in the same manner. In the DAES (Figure 5d), the spectrum corresponding to the fast component (aggregates) is more intense than that of the slow component (dimer). The reason for this difference is that at 445 nm the aggregates absorb more than the dimers and thus the aggregates' emission is more intense upon excitation at this wavelength. This finding of an amplified intensity supports the assignment of the red-shifted absorption peak to aggregates.

The existence of aggregates of **4Zn** was further verified by adding methanol and exciting at 445 nm, where the aggregates absorb more than the dimers. Three pipet drops (~36 000 equiv) of MeOH were added to the solution, and time-resolved fluorescence spectrum was recorded (Figure 5e). Again, two-component DAES gave the best fit. For excitation at 445 nm, a smaller difference in amplitude between the two components of the DAES (Figure 5f) was observed than in the situation displayed in Figure 5d. Compared to the spectrum of the solution containing no methanol (Figure 5d), the amplitude increased for

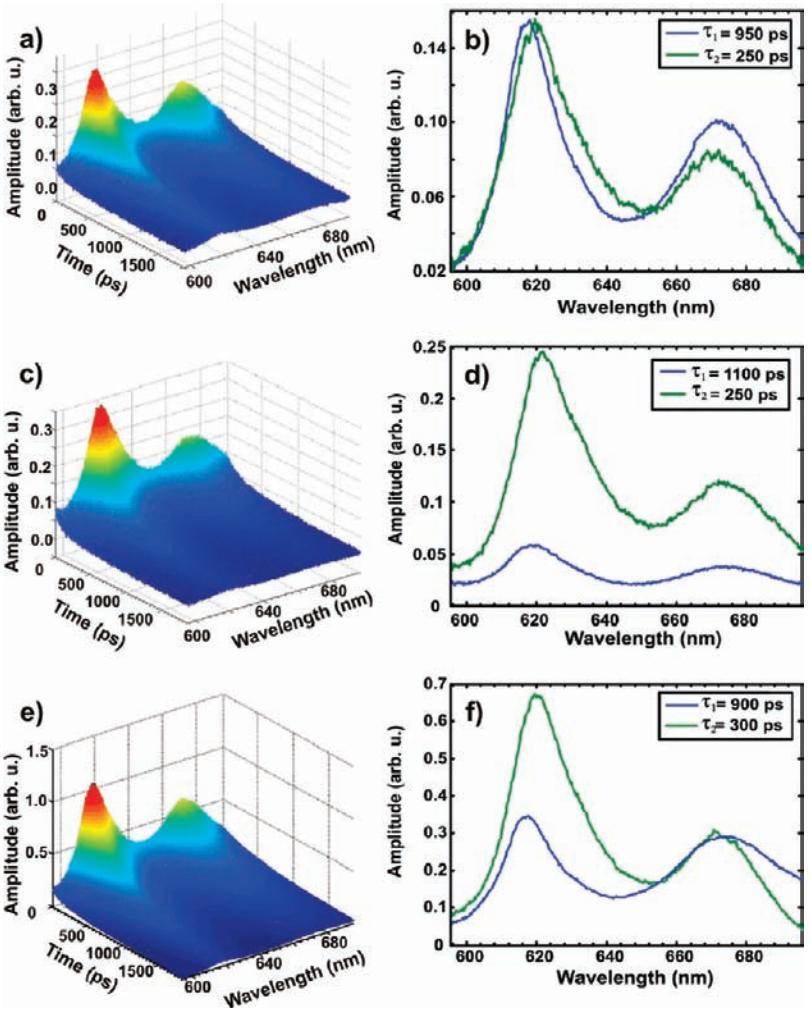

Figure 5. Time-resolved spectra (a, c, e) and their corresponding DAES (b, d, f) of **4Zn** dissolved in a minimum of CH_2Cl_2 and diluted with *n*-heptane: (a and b) λ_{ex} = 440 nm; (c and d) λ_{ex} = 445 nm; (e and f) in the presence of ~36 000 equiv of MeOH at λ_{ex} = 445 nm.

Table 1. Emission Maxima and Fluorescence Decay times

	λ_{ex} (nm)	τ_1 (ps)	τ_2 (ps)
3Zn [a]	440	700	150
	445	700	200
3Zn [a] + MeOH [b]	445	700	200
4Zn [a]	440	950	250
	445	1100	250
4Zn [a] + MeOH [b]	445	900	300
4Zn(7Zn)$_4$4Zn [c]			
concentrated	434	5160	400
dilute	434	5340	400

[a] Dissolved in CH_2Cl_2 and diluted with *n*-heptane. [b] ~36 000 equiv of MeOH. [c] Dissolved in CH_2Cl_2 and diluted with cyclohexane.

the longer decay time's DAES (dimer component). Such a presence of more dimers is expected because the addition of methanol dissociates aggregates into dimers.

Time-resolved fluorescence measurements were also performed on coordination oligomers of **7Zn** end-capped with 22.5% of **4Zn**, which corresponds to oligomers with an average formula of **4Zn(7Zn)$_4$4Zn**. Upon excitation at 434 nm, the emission maxima of **4Zn(7Zn)$_4$4Zn** were considerably red-shifted compared to those of **4Zn**. Kobuke observed similar red-shifted emission bands in self-assembled imidazolyl zinc porphyrins and attributed the red-shift to exciton interactions.[10] Two samples of different concentrations in dichloromethane—cyclohexane (Figure 6) were studied. The exact molarity of each sample was unknown; however, on the basis of the absorbance of the Soret band at 434 nm, one sample was five times more concentrated than the other. Time-resolved spectra (Figure 6a,c) were best fit by the DAES method using two different decay constants. In the more concentrated sample, decay times of 5.16 ns and 400 ps were observed (Figure 6d). These decay times are much longer than those of covalently linked multiporphyrin arrays. In general, such a significant increase can be ascribed to the delocalization of the excitation energy over several chromophores.[25] Small to moderate increases have been reported for small noncovalent cyclic species or geometrically less defined covalent species. The significant changes observed in this work suggest a more efficient delocalization along either longer or more linear species for example. Upon dilution, the shorter and longer decay times remained approximately constant (Figure 6b).

As for porphyrins **3Zn** and **4Zn**, the shorter decay time (400 ps) of **4Zn(7Zn)$_4$4Zn** was attributed to longer oligomeric species.

dx.doi.org/10.1021/ic2001255 |*Inorg. Chem.* 2011, 50, 6073–6082

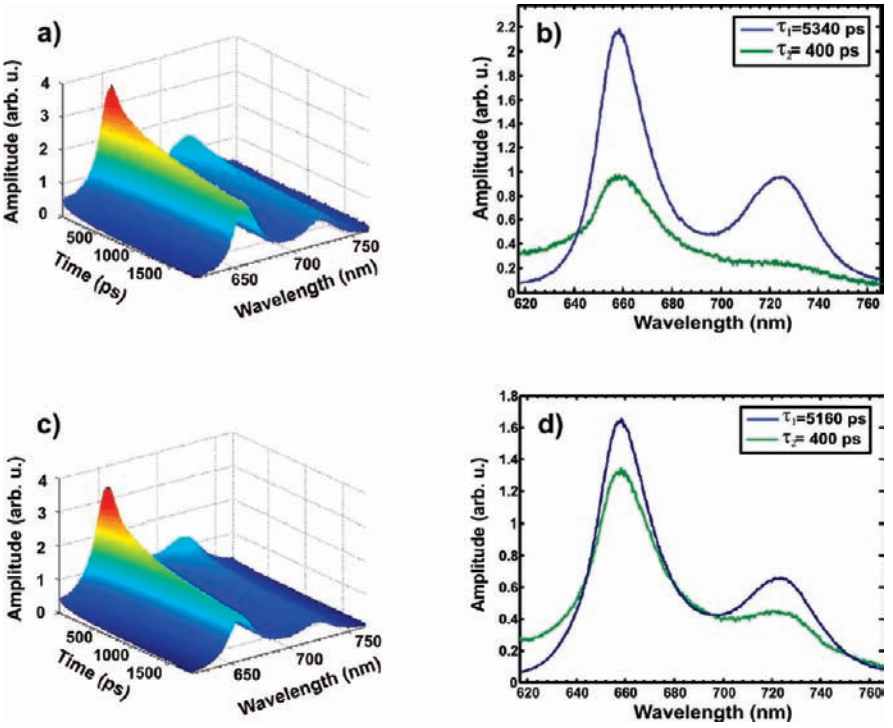

Figure 6. Time-resolved spectra (a, c) and their corresponding DAES (b, d) of **4Zn**(**7Zn**)$_4$**4Zn** in a dilute sample (a + b) and a sample five-times more concentrated (c + d). The compound was dissolved in dichloromethane and diluted with cyclohexane.

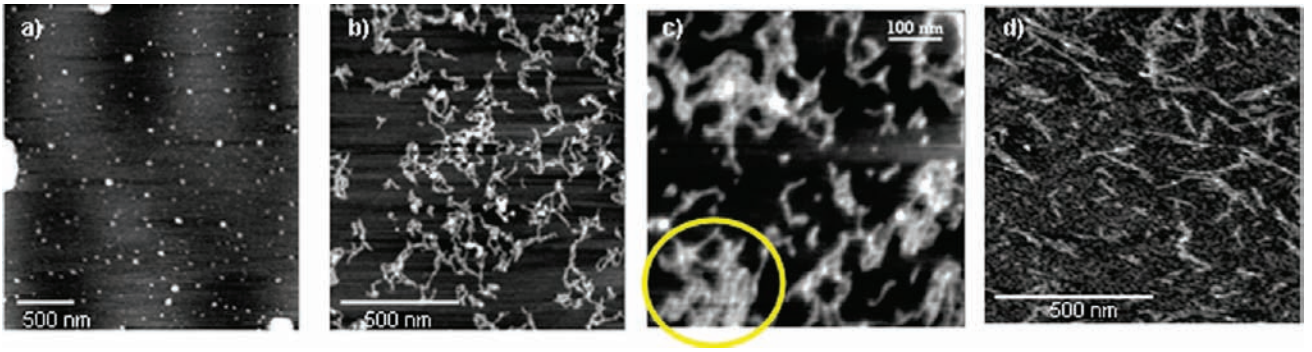

Figure 7. AFM images of **7Zn** on mica: (a) 1 μM solution of **7Zn** in THF drop-cast onto freshly cleaved mica (vertical scale = 6 nm); (b and c) 1 μM solution of **7Zn** in THF drop-cast onto mica that was first covered with a thin film of heptane [(b) vertical scale = 6 nm]; (c) close view of laterally packed chains observed on the same sample in an area of higher surface coverage density; vertical scale = 5 nm; (d) 1 μM solution of **7Zn** in pyridine drop-cast onto mica (vertical scale = 5 nm).

The amplitude of both components was nearly equal in the concentrated sample. In the more dilute sample, the associated spectrum of the longer lived component was more intense than that of the shorter lived component. The longer lived component was assigned to emission from the end caps. Thus, as intuitively expected, **7Zn** tends to form longer oligomers at higher concentration. Upon dilution, these longer species are dissociated into shorter segments.

AFM Studies of Assembly in the Solid State. Atomic force microscopy (AFM) studies were carried out to investigate the self-assembly of **7Zn** on surfaces. A rapid screening of substrates, solvents, and deposition conditions was initially conducted. Typically, 1 μM solutions of **7Zn** in $CHCl_3$, toluene, heptane, tetrahydrofuran (THF), or pyridine were prepared by diluting a 100 μM stock solution of **7Zn** in pyridine with the desired solvent. The dilute solutions were deposited on mica, HOPG, native silicon (SiO_2), or molybdenum disulfide (MoS_2) substrates by dip-coating or drop-casting. On HOPG, MoS_2, and SiO_2 substrates, ill-structured aggregates or filmlike deposits were mainly observed under the conditions tested (not shown). THF and pyridine solutions of **7Zn** led to the formation of filament-like structures on mica, as shown in Figure 7.

Drop-casting of this THF solution onto freshly cleaved mica led principally to the dispersion of **7Zn** into nonorganized aggregates on the surface, as shown in Figure 7a. However, beside the presence of some ill-defined aggregates, elongated structures were observed when the THF solution of **7Zn** was drop-cast onto mica that had first been covered with a thin film of heptane (Figure 7b,c and the Supporting Information).

dx.doi.org/10.1021/ic2001255 |*Inorg. Chem.* 2011, 50, 6073–6082

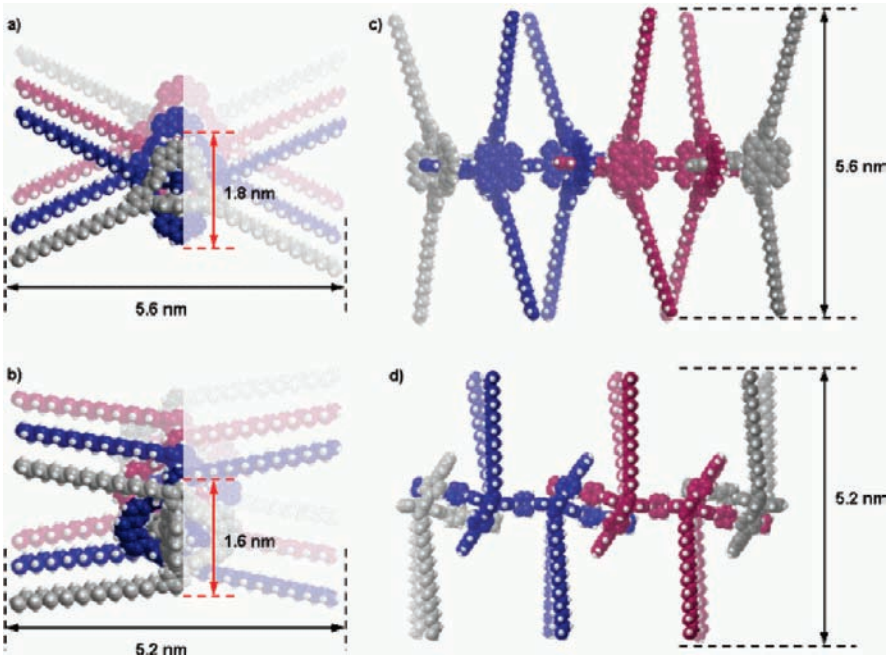

Figure 8. Space filling representation of optimized models of dimers of **7Zn** (in blue and red) including two **4Zn** end-capping units (in gray): (a and b) view along the axis of the porphyrin assembly; (c and d) bird's eye view of the assemblies. Specific dimensions are indicated for two possible orientations of the assembly on a mica surface. Model optimized on MOPAC2009 [26] using the PM6 level.[27]

The drop-casting deposition method resulted in an inhomogeneous dispersion of the material on the sample substrate's surface. In areas presenting a low surface coverage, isolated filament-like structures of homogeneous height and width were clearly observed (Supporting Information Figure S12a,b) and were attributed to isolated self-assembled porphyrin chains. These structures were sometimes decorated with small aggregates, which gave them an irregular appearance. In some cases the observation of loops and twisted structures suggested the folding of cohesive structures, i.e., chains of coordination polymers (Figure 7b and Supporting Information Figure S12a,b). In areas presenting a higher surface coverage, more complex patterns were observed; however, the filamentous nature of the underlying structures was still distinguishable even in large assemblies (Figure 7b,c and Supporting Information Figure S12c). The reproducibility of these observations was confirmed by exploring three different samples at multiple positions. Precoating the mica with heptane was found to be essential to promote the formation of such filamentous structures. It is proposed that heptane acts as a temporary passivation layer preventing the direct contact of the monomeric/oligomeric species initially present in the solution with the mica surface, thus permitting growth of the porphyrin chains before they are trapped on the surface. Further investigations are necessary to fully understand the role of the heptane layer in the self-assembly process.

The isolated filaments were 9−16 nm wide and 1.62 ± 0.52 nm high. Taking into account the radius curvature (≤10 nm) of the AFM probe, the observed widths were consistent with single strands of porphyrin assemblies. The height of the filaments does not correspond to the previously calculated and observed 1.25 nm height of the phenanthroline-strapped porphyrin from the porphyrin ring to the top of the phenanthroline strap.[14] The measured height is compatible with two possible calculated widths, as shown in Figure 8a,b. In Figure 8a, the 1.8 nm distance is measured from the top of one phenanthroline strap to the bottom of the phenanthroline strap in a second porphyrin. In this case, the porphyrins would lie parallel to the mica surface. The second calculated distance that corresponds to the measured height is the 1.6 nm width of a porphyrin between the outermost carbon atoms of the *meso*-phenyl groups (Figure 8b). In this scenario, the porphyrins would lie on their sides, perpendicular to the surface, as previously hypothesized for assemblies of dimers of **3Zn** and **4Zn** on mica.[14] The precision of the measurements does not permit discrimination between the diverse orientations possible for the porphyrin chains on the surface, and the variations observed can indicate the presence of different orientations of these chains on the mica surface.

In the area exhibiting a high density of **7Zn**, lateral association of some filament-like structures was observed, as shown in Figure 7c (circled area). In the more closely, laterally packed assemblies, a center to center distance of 6.3 ± 1.2 nm was measured between the subsequent filaments. This value is close to the theoretical widths calculated for fully extended C18 alkyl chains, i.e., 5.2−5.6 nm, as shown in Figure 8. Thus, no or very little interdigitation of the C18 alkyl chains is observed and the linear substructures most likely correspond to single strands of $(\mathbf{7Zn})_n$ chains assembled side-by-side.

Samples prepared by drop-casting of a micromolar pyridine solution of **7Zn** onto mica were more heterogeneous, presenting mostly dense films in which fibrous substructures could be distinguished (see Supporting Information). In one case isolated linear, filament-like structures were seen (Figure 7d). These structures appeared to be lying on top of a poorly organized layer of material that covered the mica surface and made it difficult to measure the height of the filament-like structures. The micromolar pyridine solution probably contained mostly monomeric or small oligomeric species due to the coordinating nature of this solvent. Therefore, the observed structures are assumed to have

dx.doi.org/10.1021/ic2001255 |*Inorg. Chem.* 2011, 50, 6073–6082

formed as the pyridine evaporated. The average, uncorrected width of the filaments was 10−15 nm, which was consistent with single stands of self-assembled **7Zn**, as described above for the THF solutions. These filaments were as long as 480 nm, which translates to 190 repeating bis(porphyrin) units for a total of 380 porphyrins. Further experiments are necessary to refine the deposition method to favor the formation of these assemblies.

CONCLUSIONS

The self-complementary imidazolyl zinc porphyrins **3Zn** and **4Zn** exist as dimers and/or J-aggregates, as demonstrated by absorption spectroscopy and time-resolved photoluminescence measurements. Assembly into linear structures was achieved with the bis(imidazolyl zinc porphyrin) **7Zn**. In organic halogenated solvents, **7Zn** self-assembles into insoluble oligomers or polymers that are at least 18 porphyrins long. Linear filaments or fibers up to 480 nm long were observed by near-field microscopy, starting from dilute pyridine solutions, in which only isolated species were present. This work demonstrates the potential of noncovalent interactions to assemble appropriately designed building blocks into long, linear structures.

EXPERIMENTAL SECTION

Calculations. Molecular mechanics calculations with the MM+ force field, semiempirical calculations at the PM3 level were performed within the HyperChem program package,[28] and semiempirical calculations at the PM6 level[27] (Figure 8) were peformed with MOPAC2009.[26] Geometry optimizations were done by alternating the molecular mechanics and semiempirical calculations, the latter providing the atomic charges used by the former without cutoffs. Convergence was usually attained for different dimers after 24 h on an IBM computer equipped with a Pentium processor and an 850 GHz clock.

Atomic Force Microscopy. AFM investigations were carried out with a commercial Nanoscope IIIa setup that controlled a Dimension 3100 scan-head (Digital Instruments, Santa Barbara, CA). All experiments were carried out in Tapping Mode under ambiant conditions. *N*-doped silicium cantilevers were used for surface imaging (NanoAndMore Gmbh): NanoSensors PointProbePlus NCH (typical tip radius, <10 nm; force constant, 42 N/m; resonance frequency, 330 kHz; back side reflex coating). For HOPG, SPI SP2 or SPI SP1 grade plates (1 × 1 cm^2) were used as supports and freshly cleaved with adhesive tape just before to use. For mica, synthetic fluorophlogopite plates (1 × 0.5 cm^2) were used. They were cut from a 1 × 1 cm^2 plate (with scissors) and cleaved with adhesive tape just before use. Images were generated using NanoScope software (version 6.14, Digital Instruments). A third-order leveling was applied to correct the pictures for the background. No other treatments were applied to the data before analysis.

Photophysical Studies. The tunable Ti:sapphire laser (Coherent, Mira) delivering sub-150 fs pulses with a repetition rate of 76 MHz was used for the excitation of the samples. To obtain an excitation within the Soret band of the investigated porphyrins (425−445 nm), the light was frequency-doubled by using beta barium borate (BBO) crystal. A combination of a spectrometer (Jobin-Yvon HR460, 100 lines/mm grating) and a streak camera (Hamamatsu C5680) was used to record the fluorescence from the samples. The streak camera was operated in the analog integration mode. The temporal and spectral resolutions of fluorescence spectra were 8 ps and 2 nm, respectively. The polarizer oriented at an angle of 54.7° relative to the polarization of the excitation was utilized to compensate for the effect of molecular rotation on the fluorescence decay. Scattered light from the excitation beam was blocked by a color glass filter (SCHOTT OG570). To minimize photodegradation during the measurement, the solutions were continuously pumped through a quartz cuvette in a closed loop. The following three-dimensional function,

$$I(\lambda, t) = \sum_{i=1}^{n} A_i(\lambda)\, e^{-t/\tau_i}$$

was used to fit the recorded data. $I(\lambda,t)$ is the wavelength λ and time t dependent experimental fluorescence intensity; A_i and τ_i are the weights and the global decay times, respectively. This applied fitting technique allows the observed fluorescence intensity to be decomposed into a sum of wavelength-dependent components A_i that each decay with wavelength-independent lifetimes τ_i. The determined set of curves $A_i(\lambda)$, called the decay-associated emission spectra, can be graphically presented to show the extracted decay times τ_i for each amplitude A_i. To compare the quality of the different DAES fits, a χ^2-value was calculated using the following formula:

$$\chi^2(\text{fit}) = \frac{1}{n_{\max} m_{\max}} \frac{1}{(I_{\text{fit,max}})^2} \left(\sum_{\text{all pixels}(n,m)} (I_{\text{signal}}(n,m) - I_{\text{fit}}(n,m))^2 \right)$$

where (n,m) is the index for the pixel map. χ^2 is normalized to the size of the pixel map ($n_{\max}m_{\max}$) and to the maximum value of the fit squared $(I_{\text{fit,max}})^2$. All presented fits had a χ^2-value below 10^{-3}.

Steady-state absorption spectra were recorded with a Varian-Cary 500 spectrophotometer.

SYNTHETIC PROCEDURES

General Method. Compounds **1**−**4**, **3Zn**, and **4Zn** were prepared according to ref 14. Reagents and solvents of reagent grade were purchased and used without further purification. Anhydrous Na_2SO_4 was used as a drying agent after aqueous workup. Evaporation and concentration in vacuo were carried out at H_2O-aspirator pressure. Column chromatography was performed with alumina from Merck (aluminum oxide 90 standardized, activity II−III according to Brockmann). Mass spectra were performed by le Service de Spectrométrie de Masse de l'Institut de Chimie, Université Louis Pasteur. Elemental analyses were performed by le Service d'Analyse Elementaire de l'Institut Universitaire de Technologie, Strasbourg, Sud, and le Service d'Analyse Elementaire de l'Institut de Chimie, Université Louis Pasteur. ^{1}H NMR spectra were recorded on Bruker Advance 300 (300 MHz) or 500 (500 MHz) spectrometers. DOSY spectra were recorded on a Bruker Avance 500 (500 MHz) spectrometer. Chemical shifts were determined by taking the solvent as a reference: $CHCl_3$ (7.26 ppm); pyridine-d_5 (7.19, 7.55, 8.71 ppm).

Synthesis of 5. To a solution of **2** (94 mg, 0.06 mmol) in THF (10 mL), zinc(II) acetate (130 mg, 0.6 mmol) was added. The mixture was stirred at 60 °C for 2 h. After evaporation of the solvent, the residue was dissolved in $CHCl_3/H_2O$ medium. The organic layer was carefully washed with water. After evaporation of $CHCl_3$, the metalated porphyrin was dried by azeotrope distillation with toluene. Crude product (quantitative yield) was used without further purification in the next step. The stoichiometry of the brominating agent was calculated on the basis of the initial quantity of free base porphyrin **2**.

To a solution of crude metalated **2** in chloroform (20 mL) was added *N*-bromosuccinimide (11 mg, 0.06 mmol). After 20 min at 0 °C, the reaction was quenched with acetone (5 mL). After evaporation of the solvent, the mixture was dissolved in CH_2Cl_2 (200 mL) and trifluoroacetic acid (10 mL) was added. The solution was stirred for 10 min at room temperature and then washed twice with 2 M Na_2CO_3(aq). The organic layer was dried over Na_2SO_4, and the solvent was removed. The mixture of porphyrins was purified by column chromatography over Al_2O_3 in CH_2Cl_2/cyclohexane (1/1) to afford **5** (97 mg, 0.06 mmol, 100%) as a glassy purple solid. mp > 250 °C. ^{1}H NMR ($CDCl_3$, 300 MHz): δ 9.61

dx.doi.org/10.1021/ic2001255 |*Inorg. Chem.* 2011, 50, 6073–6082

(d, J = 4.8 Hz, 2H), 8.97 (d, J = 4.8 Hz, 2H), 8.67 (d, J = 4.8 Hz, 2H), 8.59 (d, J = 4.8 Hz, 2H), 8.47 (br s, 1H), 8.20 (d, J = 2.6 Hz, 2H), 7.98 (d, J = 8.4 Hz, 2H), 7.81 (br s, 3H), 7.77 (d, J = 8.5 Hz, 2H), 7.54 (d, J = 8.4 Hz, 2H), 7.51 (s, 2H), 7.47 (dd, J_1 = 2.6 Hz, J_2 = 8.5 Hz, 2H), 7.20 (d, J = 1.3 Hz, 1H), 7.16 (d, J = 1.3 Hz, 1H), 6.78 (d, J = 8.4 Hz, 4H), 6.45 (d, J = 8.4 Hz, 4H), 5.54 (s, 2H), 4.28 (m, 4H), 3.67 (t, J = 7.7 Hz, 2H), 1.99 (m, 4H), 1.2−1.5 (m, 60H), 1.01 (t, J = 7.7 Hz, 2H), 0.88 (m, 6H), 0.01 (s, 9H), −2.42 (s, 2H).

Synthesis of 6. To a suspension of **5** (95 mg, 57 μmol), 1,4-diphenylboronic acid (4.35 mg, 26 μmol), and K_2CO_3 (82 mg, 0.6 mmol) in toluene (15 mL) were added water (0.3 mL) and methanol (2 mL). The mixture was Ar flushed (15 min); then $Pd(PPh_3)_4$ (5 mol %) was introduced. After degassing by bubbling the mixture with Ar for another 15 min, the reaction mixture was stirred at 60 °C for 6 h under argon. The organic phase was washed with saturated NH_4Cl(aq) (2 × 50 mL) and water (2 × 50 mL) and then dried over Na_2SO_4, filtered, and evaporated to dryness to afford a dark residue. Purification by column chromatography (Al_2O_3, C_6H_{12}/CH_2Cl_2, 1/1) was conducted in the dark to yield the SEM-protected derivative **6** (57 mg, 17 μmol, 65%) as a violet solid (second eluted product). The compound was used without further purification for the deprotection step that follows. mp > 250 °C. ^{1}H NMR ($CDCl_3$, 300 MHz): δ 9.18 (d, J = 4.5 Hz, 4H), 8.99 (d, J = 4.5 Hz, 4H), 8.87 (d, J = 4.5 Hz, 4H), 8.75 (d, J = 4.5 Hz, 4H), 8.55 (br s, 2H), 8.29 (d, J = 2.6 Hz, 4H), 8.20 (br s, 2H), 7.97 (d, J = 8.4 Hz, 4H), 7.88 (br s, 8H), 7.82 (d, J = 8.5 Hz, 4H), 7.48−7.56 (m, 12H), 7.22 (s, 2H), 7.19 (s, 2H), 6.83 (d, J = 8.2 Hz, 8H), 6.55 (d, J = 8.2 Hz, 8H), 5.59 (s, 4H), 4.29 (m, 8H), 3.71 (t, J = 8 Hz, 4H), 1.98 (m, 8H), 1.2−1.6 (m, 120H), 1.02 (t, J = 8 Hz, 8H), 0.87 (m, 12H), 0.03 (s, 18H), −2.70 (s, 4H).

Synthesis of 7. A solution of **6** (57 mg, 17 μmol) and (n-Bu_4)NF (0.1 mL of a 1 M solution in THF, 0.1 mmol) in 6 mL of THF was heated at 50 °C, in the dark, for 4 h and then poured into water. The precipitate was washed with water and dissolved in CH_2Cl_2. The organic layer was washed again with water. Solvent was removed under vacuum, and the resulting residue was dried by azeotrope distillation. Purification by column chromatography (Al_2O_3, C_6H_{12}/CH_2Cl_2, 1/1 to 0/1) was conducted in the dark to yield **7** (25 mg, 8.2 μmol, 48%) as a glassy purple solid (third eluted product). mp > 250 °C. ^{1}H NMR ($CDCl_3$, 300 MHz): δ 9.18 (d, J = 4.5 Hz, 4H), 8.99 (d, J = 4.5 Hz, 4H), 8.86 (d, J = 4.5 Hz, 4H), 8.73 (d, J = 4.5 Hz, 4H), 8.51 (br s, 2H), 8.28 (d, J = 2.6 Hz, 4H), 8.18 (br s, 2H), 7.94 (d, J = 8.5 Hz, 4H), 7.84 (br s, 2H), 7.77 (d, J = 8.6 Hz, 4H), 7.66 (br s, 6H), 7.34−7.56 (m, 16H), 6.74 (d, J = 8.4 Hz, 8H), 6.53 (d, J = 8.4 Hz, 8H), 4.26 (m, 8H), 1.96 (m, 8H), 1.56 (m, 8H), 1.2−1.5 (m, 112H), 0.83 (m, 12 H), −2.34 (s, 4H). MS. Calcd for M^+: 3061. Found: 3063.650. Anal. Calcd for $C_{212}H_{226}N_{16}O_4 + 2H_2O + 2CH_2Cl_2$: C, 78.61; H, 7.39; N, 6.38. Found: C, 78.34; H, 7.24; N, 6.00.

Synthesis of 7Zn. Zinc acetate (7.1 mg, 33 μmol) was added to a solution of **7** (10 mg, 3.3 μmol) in 5 mL of THF. The mixture was stirred at 50 °C under argon. A solid precipitated immediately. After 2 h, the mixture was poured into water. The precipitate was collected by filtration and washed thoroughly with water and then with methanol to afford **7Zn** (8 mg, 2.5 μmol, 76%) as an insoluble green material. MS MALDI TOF. Calcd for M^+: 3183.62. Found: 3183.11.

■ ASSOCIATED CONTENT

Supporting Information. Figures showing molecular modeling of dimer $(\mathbf{3Zn})_2$ or $(\mathbf{4Zn})_2$ without the alkyl chains, stick models of conformations of the out−out dimer of **3Zn** or **4Zn**, selected atomic distances in the model of the in−in dimer $(\mathbf{3Zn})_2$, COSY and NOESY NMR spectra of $(\mathbf{3Zn})_2$, time-resolved fluorescence spectra and the corresponding DAES of **3Zn**, absorption spectrum of $\mathbf{4Zn(7Zn)_4 4Zn}$, ^{1}H NMR spectrum of **7Zn** in pyridine-d_5 and of $\mathbf{4Zn(7Zn)_7 4Zn}$ in $CDCl_3$, a schematic representation of the equilibrium process of $\mathbf{4Zn(7Zn)_{m+n}4Zn}$, additional AFM images of **7Zn** on mica. This material is available free of charge via the Internet at http://pubs.acs.org.

■ AUTHOR INFORMATION

Corresponding Author

*E-mail: jweiss@unistra.fr (J.W.), jwytko@unistra.fr (J.A.W.).

Present Addresses

‡Department of Chemistry and Biochemistry, Arizona State University, P. O. Box 871604, Tempe, AZ 85287-1604, USA.

⊥Department of Chemistry, University of Saskatchewan, Saskatoon, SK S7N 5C9, Canada. On leave from the Faculty of Applied Physics and Mathematics, Gdańsk University of Technology, 80-233 Gdańsk, Poland.

■ ACKNOWLEDGMENT

We thank Prof. Jean-Pierre Bucher for providing access to an AFM instrument. M.K. thanks the Région Alsace and the CNRS for a Ph.D. fellowship. This work was supported by the CNRS (Grant ACI-NX001), the Research Council of the Université Louis Pasteur (now called the Université de Strasbourg), the DFG Research Center for Functional Nanostructures (CFN) Karlsruhe (Project C3.5), and a grant from the Ministry of Science, Research and the Arts of Baden-Württemberg (Grant No. Az. 7713.14-300). J.C. thanks the Karlsruhe School of Optics and Photonics (KSOP) for financial support.

■ REFERENCES

(1) (a) Wytko, J. A.; Weiss, J. In *N-4 Macrocyclic Metal Complexes*; Zagal, J. H., Bedioui, F., Dodelet, J. P., Eds.; Springer: Heidelberg, Germany, 2006; pp 603−724. (b) Harvey, P. D. In *The Porphyrin Handbook II*; Kadish, K. M., Smith, K. M., Guilard, R., Eds.; Academic Press: San Diego, CA, 2003; Vol. 18, Chapter 113. (c) Wolffs, M.; Hoeben, F. J. M.; Beckers, E. H. A.; Schenning, A. P. H. J.; Meijer, E. W. *J. Am. Chem. Soc.* **2005**, *127*, 13484. (d) Morisue, M.; Yamatsu, S.; Haruta, N.; Kobuke, Y. *Chem.—Eur. J.* **2005**, *11*, 5563. (e) Balaban, T. S. *Acc. Chem. Res.* **2005**, *38*, 612. (f) Lo, P.-C.; Leng, X.; Ng, D. K. P. *Coord. Chem. Rev.* **2007**, *251*, 2334.

(2) (a) Maeda, C.; Kamada, T.; Aratani, N.; Osuka, A. *Coord. Chem. Rev.* **2007**, *251*, 2743. (b) Imamura, T.; Fukushima, K. *Coord. Chem. Rev.* **2000**, *198*, 133. (c) Balaban, T. S. In *Handbook of Porphyrin Science*, Vol. 1; Kadish, K. M., Smith, K. M., Guilard, R., Eds.; World Scientific: Singapore, 2010; Vol. 1, Chapter 3.

(3) See for example:(a) Ozawa, H.; Tanaka, H.; Kawao, M.; Uno, S.; Nakazato, K. *Chem. Commun. (Cambridge, U. K.)* **2009**, 7411. (b) Xiao, S.; Myers, M.; Miao, Q.; Sanaur, S.; Pang, K.; Steigerwald, M. L.; Nuckolls, C. *Angew. Chem., Int. Ed.* **2005**, *44*, 7390. (c) Zang, L.; Che, Y.; Moore, J. S. *Acc. Chem. Res.* **2008**, *41*, 1596.

(4) Sugimoto, T.; Suzuki, T.; Shinkai, S.; Sada, K. *J. Am. Chem. Soc.* **2007**, *129*, 270.

(5) See for example: (a) Johnson, R. S.; Yamazaki, T.; Kovalenko, A.; Fenniri, H. *J. Am. Chem. Soc.* **2007**, *129*, 5735. (b) Jonkheijm, P.; Hoeben, F. J. M.; Kleppinger, R.; van Herrikhuyzen, J.; Schenning, A. P. H. J.; Meijer, E. W. *J. Am. Chem. Soc.* **2003**, *125*, 15941.

(6) Li, G.; Wang, T.; Schultz, A.; Bhosale, S.; Lauer, M.; Espindola, P.; Heinzeb, J.; Furhop, J.-H. *Chem. Commun. (Cambridge, U. K.)* **2004**, 552.

(7) Kawao, M.; Ozawa, M.; Tanaka, H.; Ogawa, T. *Thin Solid Films* **2006**, *499*, 23.

(8) (a) Yeats, A. L.; Schwab, A. D.; Massare, B.; Johnston, D. E.; Johnson, A. T.; de Paula, J. C.; Smith, W. F. *J. Phys. Chem. C* **2008**,

112, 2170, and references therein. (b) Ji, H.-X.; Hua, J.-S.; Wan, L.-J. *Chem. Commun. (Cambridge, U. K.)* **2008**, 2653.
(9) Aratani, N.; Osuka, A.; Kim, Y. H.; Jeong, D. H.; Kim, D. *Angew. Chem., Int. Ed.* **2000**, *39*, 1458.
(10) Ogawa, K.; Kobuke, Y. *Angew. Chem., Int. Ed.* **2000**, *39*, 4070.
(11) Aratani, N.; Takagi, A.; Yanagawa, Y.; Matsumoto, T.; Kawai, T.; Yoon, Z. S.; Kim, D.; Osuka, A. *Chem.—Eur. J.* **2005**, *11*, 3389.
(12) Satake, A.; Fujita, M.; Kurimoto, Y.; Kobuke, Y. *Chem. Commun. (Cambridge, U. K.)* **2009**, 1231.
(13) Koepf, M.; Trabolsi, A.; Elhabiri, M.; Wytko, J. A.; Paul, D.; Albrecht-Gary, A. M.; Weiss, J. *Org. Lett.* **2005**, *7*, 1279.
(14) Koepf, M.; Wytko, J. A.; Bucher, J.-P.; Weiss, J. *J. Am. Chem. Soc.* **2008**, *130*, 9994.
(15) Nudy, L. R.; Hutchinson, G.; Schieber, C.; Longo, F. R. *Tetrahedron* **1984**, *40*, 2359.
(16) Michelsen, U.; Hunter, C. A. *Angew. Chem., Int. Ed.* **2000**, *39*, 764.
(17) Nomoto, A.; Kobuke, Y. *Chem. Commun. (Cambridge, U. K.)* **2002**, 1104.
(18) Nomoto, A. H.; Mitsuoka, H.; Oseki, H.; Kobuke, Y. *Chem. Commun. (Cambridge, U. K.)* **2003**, 1074.
(19) Froidevaux, J.; Ochsenbein, P.; Bonin, M.; Schenk, K.; Maltese, P.; Gisselbrecht, J.-P.; Weiss, J. *J. Am. Chem. Soc.* **1997**, *119*, 12362.
(20) Paul, D.; Melin, F.; Hirtz, C.; Wytko, J.; Ochsenbein, P.; Bonin, M.; Schenk, K.; Maltese, P.; Weiss, J. *Inorg. Chem.* **2003**, *42*, 3779.
(21) Froidevaux, J. Ph.D. Thesis, Université Louis Pasteur, 1998.
(22) Huijser, A.; Marek, P. L.; Savenije, T. J.; Siebbeles, L. D. A.; Scherer, T.; Hauschild, R.; Szmytkowski, J.; Kalt, H.; Hahn, H.; Balaban, T. S. *J. Phys. Chem. C* **2007**, *111*, 11726.
(23) Yoon, M.-C.; Cho, S.; Kim, P.; Hori, T.; Aratani, N.; Osuka, A.; Kim, D. *J. Phys. Chem. B* **2009**, *113*, 15074.
(24) Leray, I.; Valeur, B.; Paul, D.; Regnier, E.; Koepf, M.; Wytko, J. A.; Boudon, C.; Weiss, J. *Photochem. Photobiol. Sci.* **2005**, *4*, 280.
(25) Yoon, Z. S.; Yang, J.; Yoo, H.; Cho, S.; Kim, D. In *Handbook of Porphyrin Science*, Vol. 1; Kadish, K. M., Smith, K. M., Guilard, R., Eds.; World Scientific: Singapore, 2010; Vol. 1, Chapter 5.
(26) Stewart, J. J. P. *MOPAC2009*; Stewart Computational Chemistry: Colorado Springs, CO, USA, 2009; http://OpenMOPAC.net.
(27) Stewart, J. J. P. *J. Mol. Model.* **2007**, *13*, 1173.
(28) *HyperChem*, Release 8; Hypercube: Gainesville, FL, 2008.